A predictive model of organic acids separation by chromatography with strong anionic resins in sulfate form

Wuyang Zhong, Patrick Perre, Fanny Duval, Julien Lemaire

A predictive model of organic acids separation by chromatography with strong anionic resins in sulfate form

Wuyang ZHONG, Patrick PERRE, Fanny DUVAL, Julien LEMAIRE*

Université Paris-Saclay, CentraleSupélec, Laboratoire de Génie des Procédés et Matériaux, SFR Condorcet FR CNRS 3417, Centre Européen de Biotechnologie et de Bioéconomie (CEBB), 3 rue des Rouges Terres 51110 Pomacle, France

* Corresponding author.

Address : CEBB,: CentraleSupélec, 3 rue des Rouges-Terres, 51110 Pomacle, France.

E-mail address: julien.lemaire@centralesupelec.fr

Tel : +33658045189

Keywords: Chromatography, Modeling, Strong anionic resin, CE/SE method, Langmuir adsorption, ion-exchange

Abstract

Organic acids commonly have quite symmetrical chromatography profiles at low pH (< 1.5) with strong anionic resins, but a significant tailing can be observed with succinic and citric acids. Classical adsorption models, like the Langmuir model, fail to predict this behavior, which can have a major influence on mean retention times and profile shapes, therefore on chromatography performances.

A new retention model was developed to better predict organic acid separation with strong anionic resin. This model combines a refined Langmuir adsorption model and an ion-exchange model. Organic acid adsorption is assumed to be due to hydrogen bonding with sulfate and hydrogen sulfate counter-anions on the resin. The adsorption capacity depends mostly on molecular size: up to sixteen formic acid molecules could be adsorbed per counter-anions, meanwhile only two succinic acid or one citric acid molecules could be adsorbed.

This adsorption model was then embedded in a generic and accurate modeling approach (continuous column with mass balance equations solved by the conservation element/solution element (CE/SE) method). All parameters of this column model were identified by fitting the simulation to experimental results (equilibrium curves and pulse tests). Then, the column model was validated with original experimental results from a binary mixture pulse test (formic and succinic acids). Results show that the simulations are much more predictive for multi-component pulse tests, both in terms of profile shape and retention time, which cannot be captured without considering ion-exchange.

Introduction

Chromatographic separation is a well-established technology in many domains, such as the food and feed industry [1], pharmaceutical production [2], protein and enzyme purification [3], and heavy metal separation [4]. Chromatography can separate or purify target components, even with very close properties like stereoisomers, without using a large amount of energy, chemicals, or solvent. For example, chromatography is often used to separate sugars or organic acids from hemicellulose hydrolysates or fermentation broths [5]. These applications often require high purity, high recovery rate, and low operational costs for economic reasons. Thus, chromatography is the ultimate solution when conventional separation techniques such as distillation, liquid-liquid extraction, membrane filtration, or crystallization are not sufficiently selective or consume too much energy, chemicals, or solvent.

Preparative chromatography consists of pushing a mixture (generally liquid) through a column filled with a porous solid phase using a mobile phase called the eluent. Its principle is to separate different compounds according to their affinities towards both phases that affect their travel speed and retention time inside the column. The solid phase can be composed of dense or microporous resin beads. Hundreds of resin types exist on the market to separate ions or organic molecules, depending on their structures and retention mechanisms. Retention of a molecule on a resin surface often implies adsorption by Van Der Waals forces owing to its hydrophobic matrix.

Ion-exchange resins are covered with counter-anions or counter-cations, making them hydrophilic [6]. For instance, molecules such as sugars or organic acids can be separated by different adsorption mechanisms (H bond, van der Waals force, chelation) with the counter-ion fixed on the resin surface, and ionic compounds can be separated by ion-exchange or Donnan exclusion effect. For example, strong anionic resins (coated with quaternary ammonium groups) or weak anionic resins (coated with amine groups) are often used to separate organic acids by interacting with their acid group.

However, the application of chromatography at an industrial scale is severely limited by its low productivity, which impacts capital expenditures, and by how it dilutes separated compounds, which impacts both capital and operational costs because further concentration steps are required. To tackle these limiting factors, several dozen multi-column chromatography processes have been developed over the last three decades, but their development and tuning are difficult. Modeling the elution profile inside columns is a valuable tool to make predictive simulations and optimize the performance of multi-column chromatography systems. Further investigations and model development are still needed to improve prediction accuracy, evidenced by continuing research activity in this field [7, 8, 9, 10].

For instance, our previous work found that outlet profiles of some organic acids have uncommon tailing that cannot be explained by usual Langmuir adsorption models [11]. This phenomenon was explained theoretically by considering the small fraction of organic acid dissociated into anions (< 1% at pH below 1.5). Historically, this fraction was neglected, but it can be strongly retained on resin ion-exchange sites [11]. A new model was then proposed to better predict the behavior of organic acids with strong anionic resins. In addition, Langmuir adsorption mechanisms were described in more detail, based on Honeywell Universal Oil Products (Honeywell UOP) patent assumptions [12]. Mono-component

simulation of an organic acid profile was performed using a discontinuous column model (Martin and Synge plate model [13]) and a finite difference method to solve differential equations. Uncommon tailing of succinic and citric acid profiles was better predicted. This model still needs to be adjusted and then validated with more experimental data and improved for multi-component simulation.

Chromatography simulation is based on solving mass balances in the mobile phase (convection-diffusion equations) and local exchanges with the stationary phase. It generally results in a non-linear and coupled system of partial differential equations. The classical numerical solving methods are finite element [14, 15, 16], finite difference [17,18], or finite volume [19] for the spatial discretization, with an explicit or implicit time scheme. The CE/SE (conservation element/solution element) method, proposed by NASA in 1995 [20], has been applied for simulating explosions [21, 22], crystallization [23] and chemical reactions [24, 25]. It was first used to simulate chromatography with the Langmuir adsorption model in 2004 [26]. The CE/SE method allows simultaneous treatment of space and time integration. In the case of packed bed chromatography [27], global trials of the CE/SE method showed a better trade-off between accuracy, stability, and calculation speed than traditional methods using an upwind scheme. Compared to conventional approaches, CE/SE method was proved, at equivalent accuracy, to save the CPU time by 77% for the pseudo-linear system of glucose-fructose separation, and by 96% for non-linear enantiomer separation [37].

The present work aims to improve the prediction of the outlet profile of different organic acids and to confirm the role of ion-exchange with strong anionic resin. A more detailed Langmuir adsorption model is proposed based on our previous theoretical work [11], assuming that adsorption is due to a hydrogen bond between organic acids and sulfate anions, as mentioned first in a UOP patent [12]. Experiments were performed first to identify all model parameters (equilibrium constant, mass transfer coefficients, axial dispersion coefficient), then to validate assumptions, and finally to check model prediction. In addition, a continuous column model, solved by the CE/SE method, was developed to more accurately simulate multi-component separation by chromatography. This new model tackles discrepancies observed in the case of succinic or citric acid separation with strong anionic resin.

2. Materials and methods

2.1 Experimental setup

The separation of organic acids by chromatography with strong anionic resin was studied using a classical chromatography setup. Experimental devices and chemicals used in this study are detailed in Tables 1 and 2.

The product or the eluent is fed at the top of column by the volumetric pump. The liquid phase flows downwards in the column, while soluble compounds interact with the resin. The output liquid goes through a pH and conductivity sensor, then a UV absorbance analyzer, and finally is sampled by a fraction collector for offline analysis. All sensors and the fraction collector are connected to a computer to monitor pH, conductivity, UV absorbance, and sample collection.

The eluent was a H_2SO_4 solution at pH 1.5 (≈ 0.02 mol/L) for all experiments. For information, its ionic strength is 0.0314 mol/L. Product pH was also adjusted at 1.5 to limit pH and conductivity variation, and to keep a similar ionic strength during coumpound elution. The

on-line measurement of UV absorbance was used to select samples to analyze by HPLC. The HPLC system (Ultimate 3000, Dionex) is equipped with a refractometer RI-101 (Shodex) at 35°C. The analytical column is an Aminex HPX-87H (Biorad) connected to a guard column (Micro-Guard cartridge Biorad) kept at 45°C within an oven. The mobile phase is a 2 mmol/L H_2SO_4 solution, prepared with Milli-Q water (Direct 8, Millipore).

The flowrate was set at 0.5 BV/h (BV represents the total bed volume, equal to 0.35 L), corresponding to 3.10^{-4} m/s interstitial flow velocity (Re_p = 6.6). The internal column diameter was 2.5 cm, and the bed length was 70 cm. A jacketed column linked to a thermostatic bath was used to maintain the temperature at 25°C. The column was filled with the strong anion resin DIAION UMA 150, functionalized with trimethylamine groups (type 1), manufactured by Mitsubishi Chemical, whose characteristics are summarized in Table 3. The resin is supplied in Cl^- form, but it was put in sulfate form before running experiments by using the following procedure: 2 BV of 1 mol/L Na_2SO_4 solution was fed into the column at 1 BV/h, then 8 BV of eluent was fed to wash the bed resin and reach pH equilibrium.

The bed porosity was measured by a pulse test with 10 mL 1 mol/L Na_2SO_4 solution eluted at 1 BV/h. The porosity was estimated between 0.39 and 0.41, which corresponds to the range given by the resin manufacturer (Table 3). Finally, the extra-column volume (in tubes, valves, sensors, etc.) was measured by performing a similar pulse test without the chromatography column. It was estimated around 0.05 BV (15 mL). All chromatographic profiles were corrected by removing this extra-column volume from the eluted volume.

2.2 Determination of transfer and axial dispersion coefficient

A pulse test consists of injecting a small volume of product (0.05 BV) followed by the eluent at a constant flow rate until all compounds leave the column. It is one of the most common methods used in chromatography to study compound retention and dispersion along the column. A pulse test was chosen in our study to determine physical properties such as adsorption isotherm, mass transfer coefficients, bed porosity and extra-column volume.

During pulse tests, component concentrations at column output are plotted as a function of the eluted volume. The curve obtained is usually called a chromatographic profile, which looks like a peak more or less wide and symmetric. This profile is mainly characterized by its mean retention volume V_R and its standard deviation σ:

$$V_R = \int_0^\infty V.c.dV \,/\, \int_0^\infty c.dV \tag{1}$$

$$\sigma^2 = \int_0^\infty V^2.c.dV \,/\, \int_0^\infty c.dV - V_R^2 \tag{2}$$

where V is the eluted volume (in BV), and c is the component concentration in the mobile phase at column output (concentration unit does not matter).

The peak width depends almost on axial dispersion and mass transfer resistance while the component passes through the column. The volume of product fed into the column (< 0.05 BV) is small enough to have a negligible influence on the shape of the pulse test profile. Dead volumes were minimized to limit their influence on dispersion. The global dispersion is usually characterized by the height equivalent to a theoretical plate (HETP) as a function of V_R, σ^2 and the bed length L:

$$HETP = \frac{L.\sigma^2}{V_R^2} \quad (3)$$

The van Deemter curve [28] describes the relationship between HETP (inversely proportional to the global dispersion) and the interstitial velocity v (in m.s^{-1}). This curve is estimated experimentally by plotting the HETP of component profiles obtained at different flowrates during the pulse test (Fig. 1).

One of the most known versions of the van Deemter equation reads as:

$$HETP = A + \frac{B}{v} + C.v \quad (4)$$

This equation considers that the global dispersion has three main causes: the mechanical dispersion (A term), the molecular diffusion (B term), and the mass transfer resistance (C term), as depicted in Figure 1. The mathematical expressions to obtain the values of A, B, and C are important for prediction purposes. The original article by van Deemter [28] gives the following expressions:

$$A = 2.\beta.d_p \qquad B = 2.\frac{D_m}{\tau} \qquad C = 2.\left[\frac{\varepsilon/\alpha}{(1+F/K_j)^2}\right] \quad (5)$$

where β is a packing factor that equals 1 for a homogeneous packed bed, d_p is the mean particle diameter (in m), D_m is the molecular diffusion coefficient (in m^2.s^{-1}), τ is the bed tortuosity, ε is the bed porosity, $F = \varepsilon/(1-\varepsilon)$ is the volumetric ratio of mobile phase to stationary phase, K_j is the linear equilibrium constant (concentration ratio between stationary and mobile phase), and α is the liquid-side local mass transfer coefficient (s^{-1}).

Within narrow operating conditions of preparative chromatography (flowrate between 0.5 and 2 BV/h), van Deemter curves are almost linear over the whole intertitial velocity range. Thus, the most simple version of van Deemter equation was sufficient to describe experimental results and estimate its coefficients.

From experimental points, the range of C can be estimated quite accurately by linear regression, then α range can be deduced from previous equation. A and B are difficult to estimate separately because of the lack of experimental points in the non-linear part of van Deemter curve. However, in the present modelling work, only axial disperion coefficient D is required, and it can be expressed as the sum of molecular diffusion and mechanical dispersion, according to the following equation:

$$D = \frac{D_m}{\tau} + \beta.d_p.v = \frac{A}{2}.v + \frac{B}{2} \quad (6)$$

Thus, the range of D can be estimated quite accurately from the experimental points by fitting the van Deemter equation with the least squares method, while considering the range of C previously estimated by linear regression.

2.3 Physical formulation at the bed level

2.3.1 Mass balance

Two types of unidimensional column model are often used to describe the mass transfer inside a chromatography column [13]:

- Continuous models, solved by usual finite methods, where the column is discretized into a large number of very small elements. In this case, the axial dispersion depends on the axial dispersion coefficient D and the global mass transfer coefficient k_a.
- Discontinuous models where the chromatography column is assimilated to a plate column. Each theoretical plate acts as a perfectly stirred reactor. In this case, the axial dispersion becomes an emerging property of the theoretical plate number N.

Discontinuous models, easy to code and to solve, require low CPU time. However, because the axial dispersion is an indirect effect of the theoretical plate number N, this model imposes the same axial dispersion for all compounds. Thus, this model is not appropriate for multi-component chromatography simulation if their axial dispersion coefficients D are not similar. That is the reason why a continuous model was chosen in the present work.

At the level of the chromatography column (Fig. 2), the local 1-D mass balance of one component j in the mobile phase, for a section of extension ∂x, can be expressed as two mass balances for liquid side and solid side:

$$\varepsilon \frac{\partial\, c_j}{\partial t} + \varepsilon . v \frac{\partial\, c_j}{\partial x} = \varepsilon . D \frac{\partial^2\, c_j}{\partial x^2} + \varepsilon . R_j^{a \leftrightarrow b} - (1-\varepsilon) . R_j^{l \leftrightarrow s} \#(7)$$

$$\frac{\partial q_j}{\partial t} = R_j^{l \leftrightarrow s} \quad (8)$$

where c_j is the concentration of component *j* in the mobile phase (in mol.m^{-3}), D is the axial dispersion coefficient (in m.s^{-2}), v is the interstitial velocity (in m.s^{-1}), $R_j^{a \leftrightarrow b}$ is the mass variation of component *j* due to acid–base reactions (in mol.m^{-3}.s^{-1}), $R_j^{l \leftrightarrow s}$ is the mass exchange of component *j* between the mobile phase and the stationary phase (in mol.m^{-3}.s^{-1}), and q_j is the concentration of component *j* in the stationary phase (in mol.m^{-3}).

The $R_j^{a \leftrightarrow b}$ term is due to the acid–base reactions in the mobile phase between SO_4^{2-} and HSO_4^- anions, organic acid HA and its conjugate base A^-, and H^+ cations. When the mobile phase goes through the column, organic acids HA can be retained by Langmuir adsorption; meanwhile, A^- can be exchanged by SO_4^{2-} or HSO_4^- anions on resin sites. As the concentration ratio between acid and basic compounds changes in the mobile phase, the acid–base reactions tend to restore equilibrium by transforming the acid into a base or the inverse.

Finally, to avoid any $R_j^{a \leftrightarrow b}$ term, mass balances in the mobile phase were written for the total content of each organic acid A ($c_A^{tot} = c_{A^-} + c_{HA}$), the total sulfate content SO_4 ($c_{SO_4}^{tot} = c_{SO_4^{2-}} + c_{HSO_4^-}$) and the total acid content H ($c_H^{tot} = c_{H^+} + c_{HA} + c_{HSO_4^-}$). These balances are not affected by acid–base reactions. Then, the concentration of each compound can be estimated using the equilibrium constant of each acid–base reaction. Indeed, these reactions are assumed to always be at an equilibrium state because they are considered to be much faster than all other phenomena.

The mass exchange $R_j^{l \leftrightarrow s}$ between the mobile phase and stationary phase depends on the adopted mass transfer model. With instantaneous mass transfer model, concentrations q_j in the stationary phase are assumed to be in equilibrium with concentrations c_j in the mobile phase. In this case, it is not necessary to estimate $R_j^{l \leftrightarrow s}$ because concentrations q_j can be deduced directly from concentrations c_j by solving the equilibrium equations system. With a

non-instantaneous mass transfer model, a new equation is needed to estimate $R_j^{l\leftrightarrow s}$, which also depends on equilibrium equations between the mobile and stationary phase.

In a previous work [11], the instantaneous mass transfer model was adopted with a discontinuous model, as the influence of mass transfer resistance can be considered directly in the theoretical plate number N that summarizes the global effect of all dispersion mechanisms.

In the present work, a non-instantaneous mass transfer model was chosen to consider compounds with different mass transfer resistances. Mass transfer resistance between the mobile and stationary phase is driven by molecular diffusion and hydrodynamic properties at the interface (summarized in the Sherwood number, depending on Reynolds and Schmidt numbers). The lumped model was chosen to estimate the mass exchange $R_j^{l\leftrightarrow s}$ from the global mass transfer coefficient k_{a_j} of component j (in s^{-1}) between the mobile phase and the stationary phase, due to diffusion inside resin and at its interface [29]:

$$R_j^{l\leftrightarrow s} = k_{a_j}.\left(q_j^{eq}(c) - q_j\right) \#(9)$$

where q_j^{eq} represents the theoretical concentration of component *j* in the stationary phase (in $mol.m^{-3}$), which would be in equilibrium with the mobile phase. This equilibrium is calculated from the concentration of all components in the mobile phase by solving all equilibrium equations (adsorption, ion-exchange, and acid–base reactions).

The mass exchange $R_j^{l\leftrightarrow s}$ can also be expressed at the liquid side, as:

$$R_j^{l\leftrightarrow s} = \alpha_j.\left(c_j - c_j^i\right) \quad (10)$$

where c_j^i is the concentration of the component j at the interface (in $mol.m^{-3}$).

Thus, k_{a_j} can be estimated from the α_j value by assuming a linear equilibrium, whose coefficient K_j is estimated from the adsorption isotherm of component j (cf. section 2.3.2).

$$q_j = K_j * c_j^i \qquad q_j^{eq} = K_j * c_j \qquad k_a = \frac{\alpha_j.\left(c_j - c_j^i\right)}{\left(q_j^{eq} - q_j\right)} = \frac{\alpha_j}{K_j} \quad (11)$$

2.3.2 Adsorption mechanisms

Counter-anions SO_4^{2-} or HSO_4^- cover the surface of strong anionic resin in sulfate form (Fig. 3). Their proportion depends on ion-exchange equilibrium and their concentration in the mobile phase. The adsorption mechanism of organic acid on this type of resin is not well documented in the literature. UOP patents [30, 31] suggested that the molecular form of organic acid was retained only on counter-anions HSO_4^- and SO_4^{2-}. Lemaire *et al*. [11] developed this hypothesis in their model, assuming that the interaction was probably hydrogen bonding between the acid hydrogen atom of organic acids and the lone electron pairs of sulfate and hydrogen sulfate oxygen atoms.

A Langmuir model is generally used to describe adsorption on chromatography resins, which involves several assumptions [32]:

1. The surface containing adsorption sites is perfectly flat with no corrugation,
2. All adsorption sites are energetically equivalent,
3. Only mono-layer coverage occurs,

4. No interaction occurs between molecules adsorbed on adjacent sites.

As shown in Figure 3, each SO_4^{2-} or HSO_4^- contains eight lone electron pairs, so up to eight hydrogen bonds can be theoretically observed on each anion. As an improvement compared to previous works [11], this feature was directly integrated into the adsorption equation in the present work. As a first approximation, the adsorption sites on SO_4^{2-} and HSO_4^- were assumed to be similar. Thus, instead of writing two adsorption equations for SO_4^{2-} and HSO_4^- separately, the total concentration of SO_4^{2-} and HSO_4^- in the stationary phase, called q_{SO4}^{tot} (in mol/L), was used. In the case of a single component model, the Langmuir equilibrium model for component *j* was described as:

$$q_j = \frac{N_{tot}.q_{SO4}^{tot}.k_{s_j}.c_j}{1 + N_j.k_{s_j}.c_j} \tag{12}$$

where N_{tot} is the number of lone electron pairs on each counter-anion ($N_{tot} = 8$), k_{s_j} is the adsorption constant of component *j,* and N_j is the number of lone electron pairs occupied by each adsorbed molecule.

In the case of a multi-component model, the competitive Langmuir equilibrium model for *m* components can be described as:

$$q_j = \frac{N_{tot}.q_{SO4}^{tot}.k_{s_j}.c_j}{1 + \sum_{i=1}^{m} N_i.k_{s_i}.c_i} \tag{13}$$

The value of q_{SO4}^{tot} can be estimated from the value of the ion-exchange resin capacity q_{max}, which is the concentration of quaternary ammonium groups RMe_3N^+. The resin supplier provides an estimation (ca. 2.3 eq/L where eq corresponds to the equivalent molar charge amount). This value was checked by mixing a given volume of resin in OH^- form with a given volume of H_2SO_4 solution whose concentration is known. The titration of residual acid concentration in the solution enabled estimating the initial OH^- concentration in resin (2.1 ± 0.2 eq/L).

Equilibrium curves of additional organic acids, determined by frontal analysis, are currently in progress in our laboratory. This dataset is intended to refine the competitive Langmuir equilibrium model. So far, these additional results are consistent and will be the object of another paper. Equilibrium curves enable us to estimate Langmuir model coefficients (N and k_s) by fitting the model to experimental points. As the N and k_s values are correlated in the linear zone of equilibrium curves, their estimation can be quite inaccurate when it is impossible to obtain sufficient experimental points in the non-linear zone. Consequently, N and k_s are given in Table 4 with their uncertainty range. Because N represents the number of lone electron pairs occupied by each adsorbed molecule, N was assumed afterward to be equal to only rounded values that could be explained physically. When the experimental range of N can include two possibilities (for formic and succinic acids), two corresponding ranges of the k_s value were identified.

According to the Langmuir adsorption model and N estimation from Table 4, formic, succinic, and citric acids seem to occupy a different number N of lone electron pairs on oxygen atoms of sulfate or hydrogen sulfate counter-anions. The values are rather consistent with their different molecular size and the number of carboxylic acid groups (Fig. 4).

Citric acid occupies more adsorption sites, most likely because of its large molecular size, which hinders access to free lone pairs, and its three carboxylic acid groups that can make H bonds with up to three lone pairs. N = 8 corresponds to only one citric acid molecule per sulfate or hydrogen sulfate counter-anion (all eight lone pairs occupied: H-bond or cluttered). Inversely, N = 0.5 or 1 for formic acid, which is the smallest acid and has only one carboxylic acid group. It corresponds to one or two formic acid molecules per lone pairs (none cluttered and only single H-bonds). The formation of formic acid dimers could explain that up to two molecules can occupy the same adsorption site [33]. Succinic acid is an intermediate case because of its medium size and two carboxylic acid groups. N = 4 or 8 corresponds to one or two succinic acids per sulfate or hydrogen sulfate counter-anions (four or eight lone pairs occupied). k_s values of formic, succinic, and citric acid are quite similar and correspond to the strength of the H-bond between their carboxylic acid group and lone electron pairs of sulfate or hydrogen sulfate counter-anions. Their value has been refined further in the present work to remove the possible influence of ion-exchange that may have caused k_s overestimation.

2.3.3 Ion-exchange mechanisms

In the present model, ion-exchange was also considered to explain the retention of some organic acids with a particular chromatographic profile (large tailing) with strong anionic resin in sulfate form. Indeed, despite the very low dissociation of organic acids at pH below 2, a small concentration of corresponding organic anions could greatly influence their profile in the case of a very strong affinity for resin ion-exchange sites.

In the mobile phase, organic acid HA and hydrogen sulfate anion HSO_4^- can dissociate into its corresponding conjugate base A^- or SO_4^{2-} and one proton H^+. The corresponding acid–base equilibria can be written as follow:

$$HA \leftrightarrow A^- + H^+ \qquad K_a^{HA} = \frac{c_{H^+}.c_{A^-}}{c_{HA}} \tag{14}$$

$$HSO_4^- \leftrightarrow {SO_4}^{2-} + H^+ \qquad K_a^{HSO_4^-} = \frac{c_{H^+}.c_{{SO_4}^{2-}}}{c_{HSO_4^-}} \tag{15}$$

In the present model, usual pKa values of formic, succinic, and citric acids and hydrogen sulfate at 20 °C (operating temperature) were considered: 3.76, 4.16, 3.13, and 1.99, respectively.

Organic anions A_j^- can replace HSO_4^- or ${SO_4}^{2-}$ counter-anions on quaternary ammonium ion-exchange sites. Ion-exchange reactions correspond to the following equilibria:

$$Me_3N^+HSO_4^- + A_j^- \leftrightarrow Me_3N^+A_j^- + HSO_4^- \qquad K^{iex}_{A_j^-/HSO_4^-} = \frac{c_{HSO_4^-}.q_{A_j^-}}{q_{HSO_4^-}.c_{A_j^-}} \tag{16}$$

$$Me_3N^+{SO_4}^{2-} + 2\,A_j^- \leftrightarrow 2\,Me_3N^+A_j^- + {SO_4}^{2-} \qquad K^{iex}_{A^-/{SO_4}^{2-}} = \frac{c_{{SO_4}^{2-}}.{q_{A_j^-}}^2}{q_{{SO_4}^{2-}}.{c_{A_j^-}}^2} \tag{17}$$

$$Me_3N^+{SO_4}^{2-} + 2\,HSO_4^- \leftrightarrow 2\,Me_3N^+HSO_4^- + {SO_4}^{2-} \qquad K^{iex}_{HSO_4^-/{SO_4}^{2-}} = \frac{c_{{SO_4}^{2-}}.{q_{HSO_4^-}}^2}{q_{{SO_4}^{2-}}.{c_{HSO_4^-}}^2} \tag{18}$$

where $K^{iex}_{X^-/Y^-}$ is the ion-exchange coefficient of anions X^- by anions Y^- on resin sites.

In the stationary phase, the concentration of ion-exchange sites q_{max} is always conserved:

$$q_{max} = 2.q_{SO_4{}^{2-}} + q_{HSO_4{}^-} + \sum_j q_{A_j^-} \quad (19)$$

All corresponding equilibrium constants can be deduced from resin manufacturer data listed in the appendices [34, 35], which provides the value of $K^{eq}_{X^-/OH^-}$ between many anions X^- and OH^-.

2.4 Computational strategy

As detailed in the introduction, several computational methods could be used to solve the system of equations in space and in time. The CE/SE method was chosen in the present work for its ability to deal with space and time integrals simultaneously. The integral is calculated between normal mesh points and intermediate mesh points, and it takes two integrals to move one step forward in space or time.

This method is based on Gauss's divergence theorem [36]. In the case of a 1D space model, it is also called Green's theorem. For a partial differential equation (PDE) like:

$$\frac{\partial u}{\partial t} + \frac{\partial f}{\partial x} = p \quad (20)$$

Green's theorem tells us that the line integral along a closed curve ∂C of a function equals the integral of the derivative over the corresponding plane region ∂D:

$$\oint_{\partial C} (-u.dx + f.dt) = \iint_{\partial D} \left(\frac{\partial u}{\partial t} + \frac{\partial f}{\partial x}\right).dx.dt = \iint_{\partial D} p.dx.dt \quad (21)$$

Figure 5 shows the space and time discretization used and the mesh points where all variables are estimated. By definition, the solution element SE (j,n) is the gray space-time interior region centered at point A (j,n). It includes a horizontal line segment, a vertical line segment, and their immediate neighborhood points (B, D, F). In this solution element, we chose to approximate u and f values by a first-order Taylor formula from its center point A (j,n):

$$u^*(x,t) \sim u_j^n + u_{x_j}{}^n.(x - x_j) + u_{t_j}{}^n.(t - t_n) \quad (22)$$

$$f^*(x,t) \sim f_j^n + f_{x_j}{}^n.(x - x_j) + f_{t_j}{}^n.(t - t_n) \quad (23)$$

where u_{xj}^n and f_{xj}^n correspond to the space derivative of u and f at the mesh point (j,n), and u_{tj}^n and f_{tj}^n correspond to the time derivative of u and f at the mesh point (j,n).

A zero-order Taylor formula was chosen to approximate the source term p, which means that p was treated as a constant in each solution element:

$$p^*(x,t) \sim p_j^n \quad (24)$$

The conservation element CE (j,n) corresponds to the rectangle FADE (blue) and ABCD (green), where the source term p was consequently considered equal at mesh points A, B, D, and F, but different at mesh points C ($p_{j-1/2}^{n-1/2}$) and E ($p_{j+1/2}^{n-1/2}$).

Finally, Green's theorem applied within the rectangle FBCE (blue + green) by approximating u, f and p leads to the following explicit equation that enabled u_j^n to be estimated from values of u, f and p at the previous semi-time step:

$$u_j^n = \frac{1}{2}\left[u_{j+\frac{1}{2}}^{n-\frac{1}{2}} + u_{j-\frac{1}{2}}^{n-\frac{1}{2}}\right] - s_{j+\frac{1}{2}}^{n-\frac{1}{2}} + s_{j-\frac{1}{2}}^{n-\frac{1}{2}} + \frac{\Delta t}{4}.\left(p_{j+\frac{1}{2}}^{n-\frac{1}{2}} + p_{j-\frac{1}{2}}^{n-\frac{1}{2}}\right) \quad (25)$$

where

$$s_{j\pm\frac{1}{2}}^{n-\frac{1}{2}} = \left(\frac{\Delta t}{2.\Delta x}\right).f_{j\pm\frac{1}{2}}^{n-\frac{1}{2}} + \left(\frac{\Delta x}{8}\right).u_{x_{j\pm\frac{1}{2}}}^{n-\frac{1}{2}} + \left(\frac{\Delta t^2}{8.\Delta x}\right).f_{t_{j\pm\frac{1}{2}}}^{n-\frac{1}{2}} \quad (26)$$

In the case of chromatography convection-diffusion equation, the CE/SE method can be applied to solve the mass balance in the mobile phase by defining:

$$f = v.c - D.\frac{\partial c}{\partial x} \qquad u = c \qquad p = -\frac{(1-\varepsilon)}{\varepsilon}.k_a.(q^{eq} - q) \quad (27)$$

As a consequence, f, u_t, f_x, then f_t can be deduced from u_x at the mesh point (j,n):

$$f = v.u - D.u_x \qquad f_x = \frac{\partial f}{\partial u}.\frac{\partial u}{\partial x} = \left(v.\frac{\partial u}{\partial u} - D.\frac{\partial u}{\partial u \partial x}\right)u_x \sim v.u_x \quad (28)$$

$u_t = p - f_x$ (Eq 20) $\qquad f_t = \frac{\partial f}{\partial u}.\frac{\partial u}{\partial t} = \left(v.\frac{\partial u}{\partial u} - D.\frac{\partial u}{\partial u \partial x}\right)u_t \sim v.u_t \quad (29)$

This set of equations prove that only u and u_x are needed to solve Eq 25. There are many possibilities to calculate the derivative u_x from u. In the present model, it was calculated by using a modified harmonic mean [37]:

$$u_x = \frac{|u_x^+|u_x^- + |u_x^-|u_x^+}{|u_x^+| + |u_x^-|} \qquad u_x^- = \left(u_j^n - u_{j-1}^n\right)/\Delta x \qquad u_x^+ = \left(u_{j+1}^n - u_j^n\right)/\Delta x \quad (30)$$

where u_x^- and u_x^+ are the partial derivatives on the left and right sides, respectively. The modified harmonic mean equals zero when u_x^- and u_x^+ have opposite signs and equals the traditional harmonic mean when u_x^- and u_x^+ have the same sign.

Thus, only one variable u is needed to solve the system, which is calculated via Eq 25 with an explicit scheme. Starting from points at time step n, Eqs 22–30 allow us to move to time step n+1/2. Points at time n+1 are then calculated in the same way as points at time n+1/2.

Meanwhile, the mass balance in the stationary phase can be solved separately by a 1st order finite-difference method, at each mesh point (j,n):

$$\frac{q_j^n - q_j^{n-1}}{\Delta t} = k_a.\left(q^{eq}{}_j^n - q_j^n\right) \quad (31)$$

Boundary conditions are used to obtain values of first and last mesh points, as proposed by Chuanyi et al. [37]:

$$\frac{\partial c_1^n}{\partial x} \sim \frac{c_2^n - c_1^n}{\Delta x} = \frac{v}{D}\left(c_1^n - c_{feed}\right) \quad (32)$$

$$\frac{\partial c_{j_{end}}^n}{\partial x} \sim \frac{c_{j_{end}}^n - c_{(j_{end}-1)}^n}{\Delta x} = 0 \quad (33)$$

3. Results and discussion

3.1 Influence of Langmuir and ion-exchange coefficients

A tailing can be observed in the chromatography outlet profile of some organic acids with a strong anionic exchange resin. Theoretically, this could be due to a high value of their adsorption affinity k_s or ion-exchange coefficient K^{iex}. Figures 6-A and 6-B show the impact of values k_s and K^{iex} on the outlet profile during the single component pulse test simulation of citric acid with parameters of Tables 4, 5 and 7. In Figure 6-A, K^{iex} is fixed at 1, a negligible value, to study only the influence of k_s on the profile shape and position. Then, the influence of K^{iex} is depicted in Figure 6-B. Pulse tests with different values of K^{eix} were simulated. As the objective was to highlight the effect of K^{iex} only on the profile shape, the value of k_s was adjusted for each value of K^{iex} to obtain the same retention volume.

As expected, Figure 6-A shows that the higher is the adsorption coefficient k_s, the higher is the retention volume. However, the value of the coefficient k_s barely changes the profile shape and its relative symmetry. In comparison, Figure 6-B shows that K^{iex} significantly impacts the profile shape by increasing its tailing.

To summarize, the retention volume depends on both K^{iex} and $\mathrm{k_s}$ while the profile tail is influenced almost solely by K^{iex}. Indeed, very high k_s values could also lead theoretically to significant profile tailing, but these values would not be consistent with experimental retention volume, which corresponds to a k_s ranging between 0 and 0.3 L/mol.

The impact of ion-exchange constant K^{iex} depends on the pH of the liquid phase and the pKa of the organic acid. When the pH is much lower than pKa (pH < pKa - 2), organic acids are mainly in molecular form. In this case, a very small proportion is dissociated into the anionic form, and the peak is less sensitive to the value of K^{iex}.

3.2 Identification of Langmuir and ion-exchange coefficients

In the present study, K^{iex} was estimated to reproduce the experimental profile tailing obtained for formic, succinic, and citric acids, starting from the resin supplier's estimation. Meanwhile, k_s was adjusted to fit the experimental retention volume. Initially, k_s was set to the experimental value estimated previously from equilibrium curves, considering different possible N values (Table 4). Figure 7 shows experimental mono-component pulse tests that were used to refine estimations of k_s and K^{iex} given in Table 6. The operating conditions of these pulse tests are detailed in Table 5.

The mean value of D obtained from the van Deemter curve was used for simulation. Only the value of k_a was slightly adjusted to fit better the peak left front (Table 7).

In Table 6, the identified ranges of K^{iex} correspond quite well to the supplier's data for formic and citric acids. k_s ranges identified from pulse test simulations were not influenced by different possible N values considered for each organic acid. Indeed, the denominator $(1 + N.k_s.c)$ of the Langmuir equation remained close to 1 because of weak component concentration during pulse test simulations. For formic and succinic acids, the k_s range estimated from pulse test simulation is consistent with its range identified from equilibrium curves, for N = 0.5 and 4, respectively. Meanwhile, the k_s range of citric acid identified from pulse tests lies at the bottom of its range estimated from equilibrium curves. Thus, 0.5, 4 and 8 were considered afterward as the unique, consistent N values for formic, succinic and citric acids, respectively. For citric acid, the slight k_s overestimation from equilibrium curves

can be explained by the strong influence of ion-exchange (illustrated by the significant tailing of the citric acid profile, cf. Fig. 7).

3.3 Analysis of ion-exchange effect on the chromatography profile

Figure 7 presents simulation curves of pulse tests for different organic acids, to compare the Langmuir adsorption model with the hybrid model, which considers that organic acid can be retained by Langmuir adsorption but also by ion-exchange.

Both models can predict the experimental results for formic acid. This is not surprising as its tailing is negligible, and its profile is almost symmetrical. The formic acid profile is marginally influenced by ion-exchange due to its very low K^{iex} (< 30). Moreover, it is much less dissociated into anions than citric acid because of its higher pKa (3.76 vs. 3.13). Thus, at pH 1.5, only 0.5% formic acid is dissociated, making the ion-exchange effect even more negligible.

In comparison, succinic acid has the highest pKa (4.16) but also the highest K^{iex} according to Table 6 (900 ± 100). Therefore, despite a low proportion dissociated into anions (0.2% at pH 1.5), the strong retention of succinate anion on resin ion-exchange sites can explain its slight profile tailing.

Finally, the citric acid profile has the largest tailing because of its lower pKa (3.13) and quite high K^{iex}. Indeed, citric acid is the most dissociated into anions (2.3% at pH 1.5) and citrate anions are strongly retained by ion-exchange.

Figure 7 confirms that the tailing of succinic and citric acid profiles cannot be reproduced by the Langmuir adsorption model. In contrast, the hybrid model is in good agreement with experimental results. It confirms that organic anions retention by ion-exchange must be considered to make predictive simulation, even if they are poorly dissociated at pH = 1.5.

4. Multi-component pulse test prediction

To confirm that the hybrid model is more predictive than the model with only Langmuir adsorption, a pulse test with a mixture of formic acid and succinic acid was both simulated and carried out (Fig. 8). Table 8 gives parameter values used in both models, whose ranges were estimated previously from experimental data analysis (Tables 6 and 7).

Experimental profiles depicted in Figure 10 correspond to a pulse test performed with 10 mL pH 1.5 solution, composed of 0.65 mol/L formic acid and 0.267 mol/L succinic acid, eluted with pH 1.5 H_2SO_4 solution at 0.5 BV/h, using the same setup described above.

Figure 8 confirms clearly that the hybrid model predicts the chromatographic profile of both organic acids much better. More specifically, the hybrid model is able to predict the significant tailing of the succinic acid profile, unlike the Langmuir model. Moreover, the mean retention volume of formic acid is better predicted by the hybrid model, even though there is still a slight difference (0.1 BV) compared to experimental points.

The slight discrepancies observed can be due to assumptions and simplifications in the present hybrid model. For example, all adsorption sites were considered equivalent. To be more accurate, adsorption sites on the upper side of ${SO_4}^{2-}$ and ${HSO_4}^{-}$ counter-anions should be considered more accessible than sites closer to the resin matrix (Fig. 4). In addition, some studies [38, 39] showed that the original Langmuir competitive equation is

not suitable for multi-layer adsorption. Thus, a more accurate model considering different types of adsorption sites might be an interesting approach to better predictions of multi-component mixture separation by chromatography.

5. Conclusion

Strong anionic resins, often used in sulfate form in chemical or food and feed industries to separate organic acids by chromatography, require better retention mechanisms to improve the model's prediction. In this work, a hybrid model was developed and used to explain the elution profiles of succinic and citric acids, which display unusual tailing. Compared to classic Langmuir adsorption models, it also considers the effect of organic acid dissociation into anions that can be retained on resin ion-exchange sites. The model was solved with the CE/SE method.

Estimation of adsorption equilibrium coefficient (N and k_s) were consistent with the adsorption of organic acids by means of hydrogen bonding between the hydrogen atom of the carboxylic acid group and one lone electron pair of oxygen atoms of sulfate or hydrogen sulfate counter-anions. Present results confirm that the tailing of succinic and citric acid profiles is mainly caused by ion-exchange of their very low dissociated fraction, even at low pH (< 1.5). Organic acid dissociation and ion-exchange is, therefore, must be considered to develop a predictive model for succinic and citric acids. The prediction of the hybrid model was successfully validated in the case of a multi-component pulse test.

This hybrid model is currently implemented in a multi-column chromatography simulation program to predict and optimize the performance of simulated moving bed technologies. It is also useful to design new multi-fraction processes.

Acknowledgments

This study was carried out in the Centre Européen de Biotechnologie et de Bioéconomie (CEBB), supported by Région Grand Est, Département de la Marne, Grand Reims and the European Union. In particular, the authors would like to thank Département de la Marne, Grand Reims, Région Grand Est and European Union with European Regional Development Fund (ERDF Champagne-Ardenne 2014-2020) for their financial support to the Chair of Biotechnology of CentraleSupélec.

References

[1] Jun Y., Feijie H., Wenyan H., Method for detecting paraffin in food by gas chromatography and gas chromatography-mass spectrometry and application thereof, Worldwide applications, CN Patent 102621245A, 2012

[2] Shane M.P., Methods for monitoring integrated continuous pharmaceutical manufacturing processes, US Patent 20160041551A1, 2016,

[3] Qiao-Le H., Zhao-xi S., Liming Z., Model-based process design of a ternary protein separation using multi-step gradient ion-exchange SMB chromatography, Computers & Chemical Engineering 138 (2020), https://doi.org/10.1016/j.compchemeng.-2020.106851

[4] Ammann, A.A. Speciation of heavy metals in environmental water by ion chromatography coupled to ICP–MS, Anal Bioanal Chem 372 (2002), 448–452, https://doi.org/10.1007/s00216-001-1115-8

[5] Kaifei C., Shilai H., Hang L., Gang L., Shicheng Z.g, Jian-min C., Ion exchange separation for recovery of monosaccharides, organic acids and phenolic compounds from hydrolysates of lignocellulosic biomass, Separation and Purification Technology 172 (2017), 100-106, https://doi.org/10.1016/j.seppur.-2016.08.004

[6] Bolin G., Lili W., Chaozhan W., Xindu G., Preparation of hydrophobic interaction chromatographic packings based on monodisperse poly (glycidyl-methacrylate-co-ethylenedimethacrylate) beads and their application, Journal of Chromatography A 1022 (2004), 33-39 https://doi.org/10.1016/j.chroma.-2003.09.063

[7] Shanshan S., Xiulan X., Lijun Z., Liang C., Zhaochu X., Yufeng L., Preparative separation of five polyphenols from the fruits of Sorbus pohuashanensis Hedl. by high-speed counter-current chromatography, Journal of Chromatography B 1172 (2021), https://doi.org/10.1016/j.jchromb.2021.122620.

[8] Ton B., Pascal B., Peter J.S., Ron A.H. Peters, Charge-based separation of synthetic macromolecules by non-aqueous ion exchange chromatography, Journal of Chromatography A 1626 (2020), https://doi.org/-10.1016/j.chroma.2020.461351.

[9] Ali S., Mohammad Reza K., Masoud A., Ahmad S., Shahram S., Mathematical modeling and optimization of industrial scale ELUXYL simulated moving bed (SMB), Separation and Purification Technology 248 (2020), https://doi.org/10.1016/-j.seppur.2020.116961.

[10] Cheol-Yeon J., Jae-Hwan C., Jin-Woo K., Sungyong M., Development of a simulated moving bed process for ultra-high-purity separation of ribose from a low-selectivity sugar mixture in microalgal hydrolyzate, Separation and Purification Technology 262 (2021), https://doi.org/10.1016/-j.seppur.2020.118298

[11] Julien L., Claire-Line B., Florence L., Marc-André T., Moncef S., Dominique P., Purification of organic acids by chromatography with strong anionic resins: Investigation of uptake mechanisms; Journal of Chromatography A 1458 (2016), 63-69, https://doi.org/10.1016/j.chroma.-2016.06.057.

[12] Kulprathipanja S., Oroskar A.R., Separation of lactic acid from fermentation broth with an anionic polymeric absorbent, US Patent 5068418, 1991.

[13] Guiochon G., Shirazi D.G., Felinger A., Katti A.M., Fundamentals of preparative and non-linear chromatography, Academic Press 2nd edition (2006), 283–286, ISBN0123705371, 9780123705372.

[14] Juke, A., Epping, A., Schmidt-Traub, H., Optimal design of batch and simulated moving bed chromatographic separation processes, Journal of Chromatography A 944 (2012), 93-117, https://doi.org-/10.1016/S0021-9673(01)01311-5.

[15] Kaczmarski K., Use of orthogonal collocation on finite elements with moving boundaries in the simulation of non-linear multi-component chromatography. Influence of fluid velocity variation on retention time in LC and HPLC, Computers & Chemical Engineering 20 (1996), 49-64, https://doi.org/10.1016/0098-1354(95)00004-L.

[16] Hørsholt A., Christiansen L.H., Meyer K., Huusom J.K., Jørgensen J.B., A Discontinuous-Galerkin Finite-element method for simulation of packed bed chromatographic processes, FAC-PapersOnLine 52 (2019), 346-351, https://doi.org/10.1016/-j.ifacol.2019.06.086.

[17] Dünnebier G., Weirich I., Klat K.U.t, Computationally efficient dynamic modelling and simulation of simulated moving bed chromatographic processes with linear isotherms, Chemical Engineering Science 53 (1998), 2537-2546, https://doi.org/10.1016/S0009-2509(98)00076-1.

[18] Kaczmarski K., Antos D., Fast finite difference method for solving multi-component adsorption-chromatography models, Computers & Chemical Engineering 20 (1996), 1271-1276, https://doi.org/10.1016-/0098-1354(95)00247-2.

[19] Lim Y.I., Le Lann J.M., Joulia X., Accuracy, temporal performance and stability comparisons of discretization methods for the solution of partial differential equations (PDEs) in the presence of steep moving fronts, Computers and Chemical Engineering, 25 (2001), 1483-1492, https://doi.org/10.1016/S0098-1354(01)00712-8.

[20] Chang, S.C., The method of space-time conservation element and solution element—A new approach for solving the navier-stokes and euler equations. J. Comput. Phys. 119, 2 (July 1995), 295–324. https://doi.org/10.1006/-jcph.1995.1137

[21] Wei L., Dong H., Pan H., Hu X., Zhu J., Study on the mechanism of the deflagration to detonation transition process of explosive, Journal of Energetic Materials 32 (2014) 238-251. https://doi.org/10.1080/07370652.2013.825347

[22] Shen H., Gang W., Liu K., Deliang Z. Numerical simulation of liquid-fueled detonations by an eulerian-lagrangian model. International Journal of Nonlinear Sciences and Numerical Simulation (2012), 13, https://doi.org/177-188. 10.1515/ijnsns.2011.102.

[23] Orkomi A.A., Shahrokhi M., Simulation and control of multidimensional crystallization processes, Chem. Eng. Commun. 201 (2014), 870-895, https://doi.org/10.1080-/00986445.2013.785947.

[24] Qamar S., Yousaf M., The space-time CESE method for solving special relativistic hydrodynamic equations, J. Comput. Phys. 231 (2012) 3928-3945, https://doi.org/-10.1016/j.jcp.2012.01.039.

[25] Sadighi S., Ahmad A., Shirvani M., Dynamic simulation of a pilot scale vacuum gas oil hydrocracking unit by the space-time CE/SE method, Chemical Engineering & Technology 35 (2012), 919-928, https://doi.org/10.1002/ceat.201100305

[26] Young-Il L., Sten-Bay J., A fast and accurate numerical method for solving simulated moving bed (SMB) chromatographic separation problems, Chemical Engineering Science, Volume 59 (2004), 1931-1947, https://doi.org/10.1016-/j.ces.2003.12.026

[27] Lan L., Young-Il L., Performance evaluation of the conservation element and solution element method in SMB process simulation; Chemical Engineering and Processing 48 (2009), 878–884, https://doi.org/10.1016/j.cep.2008.11.003

[28] Van Deemter J. J., Zuiderweg F.J., Klinkenberg A., Longitudinal diffusion and resistance to mass transfer as causes of nonideality in chromatography. Chemical Engineering Science 50 (1995), 3869-3882, https://doi.org/10.1016/00092509-(96)81813-6.

[29] Felinger, A., Guiochon, G. Comparison of the kinetic models of linear chromatography. Chromatographia 60 (2004), 175-180. https://doi.org/10.1365-/s10337-004-0288-7

[30] Kulprathipanja S., Oroskar A.R., Separation of lactic acid from fermentation broth with an anionic polymeric absorbent, US Patent 5068418, 1991.

[31] Kulprathipanja S., Oroskar A.R., Separation of an organic acid from fermentation broth with an anionic polymeric adsorbent, US Patent 5068419,1991.

[32] Sircar S., Comments on practical use of Langmuir gas adsorption isotherm model. Adsorption 23 (2017), 121–130. https://doi.org/10.1007/s10450-016-9839-0
[33] Benni D., Weichao Z., Catalytic effect of water, water dimer, or formic acid on the tautomerization of nitroguanidine, Computational and Theoretical Chemistry 1049 (2014), 90-96, https://doi.org/10.1016/-j.comptc.2014.09.025.
[34] Ion Exchange Resins Selectivity, DuPont, Form No. 45-D01458-en, Rev. 2 November 2019
[35] DOWEX™ Ion Exchange Resins Technical Information, Form No. 177-01755-0207
[36] Sin-Chung C., "Courant Number and Mach Number Insensitive CE/SE Euler Solvers," AIAA Paper 2005-4355, 41st AIAA/ASME/SAE/ASEE Joint Propulsion Conference and Exhibit (2005), Tucson, AZ.
[37] Chuanyi Y., Shaokun T., Yinghua L., Hong-Mei Y., Moses O.T., Combination of space–time conservation element/solution element method and continuous prediction technique for accelerated simulation of simulated moving bed chromatography, Chemical Engineering and Processing: Process Intensification 96 (2015), 54-61, https://doi.org/10.1016/-j.cep.2015.07.023.
[38] Neil R.A., Adsorption of formic acid on clean and oxygen covered Pt(111), Applications of Surface Science 11-12 (1982), 774-783, https://doi.org/10.1016/0378-5963(82)90120-9.
[39] Nejad A., Suhm M., Concerted Pair Motion Due to Double Hydrogen Bonding: The Formic Acid Dimer Case, Journal of the Indian Institute of Science 100 (2019), https://doi.org/100. 10.1007/s41745-019-00137-5.

Appendices

SBA (strong base anion) resins selectivity coefficients [34, 35]

Anion	Type 1	Type 2
$HSiO_3^-$	<1.0	<1.0
OH^-	1.0	1.0
F^-	1.6	0.3
$CH_3CH_2COO^-$	2.6	0.3
CH_3COO^-	3.2	0.5
$HCOO^-$	4.6	0.5
$H_2PO_4^-$	5.0	0.5
IO_3^-	5.5	0.5
HCO_3^-	6.0	1.2
Cl^-	22	2.3
NO_2^-	24	3
BrO_3^-	27	3
HSO_3^-	27	3
CN^-	28	3
HSO_4^-	35	9
Br^-	50	6
NO_3^-	65	8
ClO_3^-	74	12
Phenate	110	27
SO_4^{2-}	150	/
I^-	175	17
SeO_4^{2-}	280	/
Citrate	220	23
ClO_4^-	>500	/
CrO_4^{2-}	1700	/
$C_6H_5SO_3^-$	>500	75

Figures and Tables

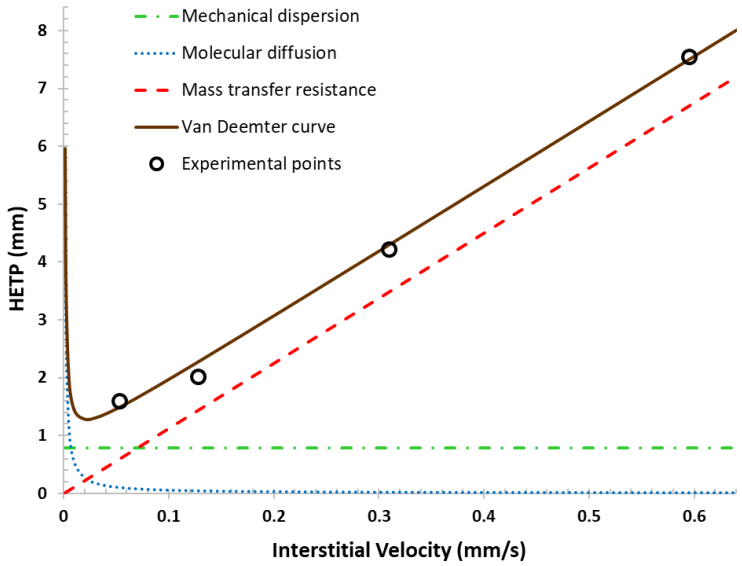

Fig. 1. van Deemter Curve of succinic acid eluted with H_2SO_4 solution at pH 1.5 with the system described in materials and methods.

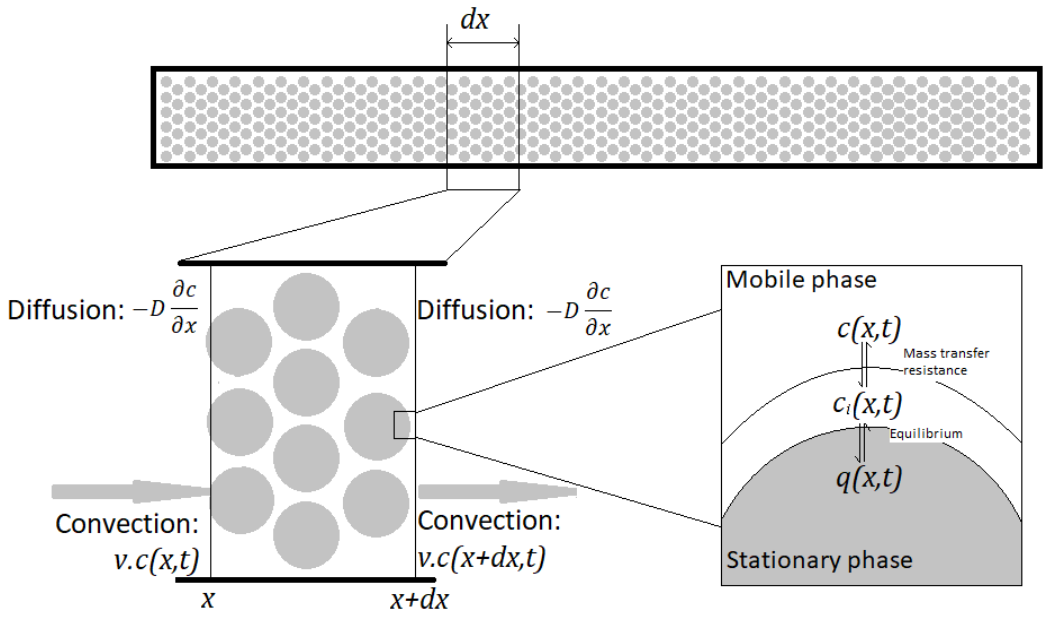

Fig. 2. Mass balance (convection-diffusion equation) and mass transfer model

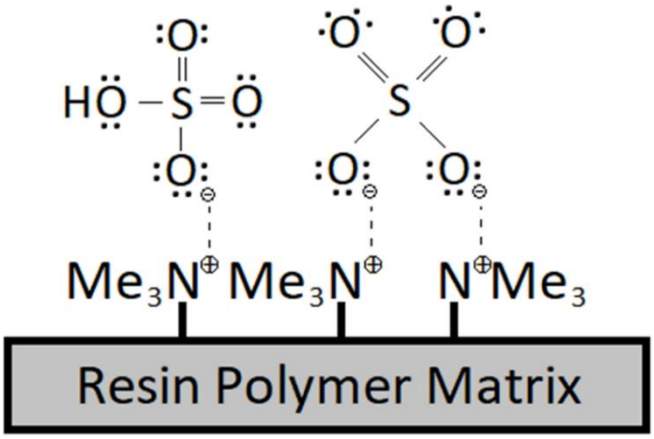

Fig. 3. Schematical representation of the strong anion resin (type 1) in sulfate form.

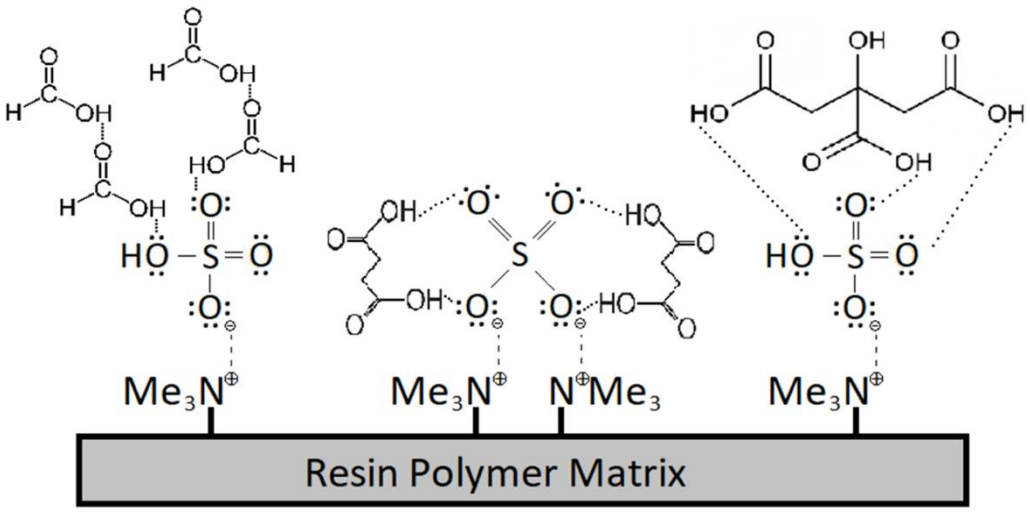

Fig. 4. Schematic illustration of organic acid adsorption by hydrogen bonding on SO_4^{2-} or HSO_4^- counter-anions, which have eight lone electron pairs each. N = 0.5 for formic acid could be explained by dimer conformation, and means that up to 16 molecules could be adsorbed (only 4 of them are represented). N = 8 for citric acid corresponds to one molecule maximum adsorbed on each counter-anion. Indeed, citric acid can form up to 3 hydrogen bonds and the other five free sites could be cluttered. N = 4 for succinic acid corresponds to 2 molecules maximum adsorbed on each counter-anion, because it can form up to 2 hydrogen bonds and could clutter less free sites.

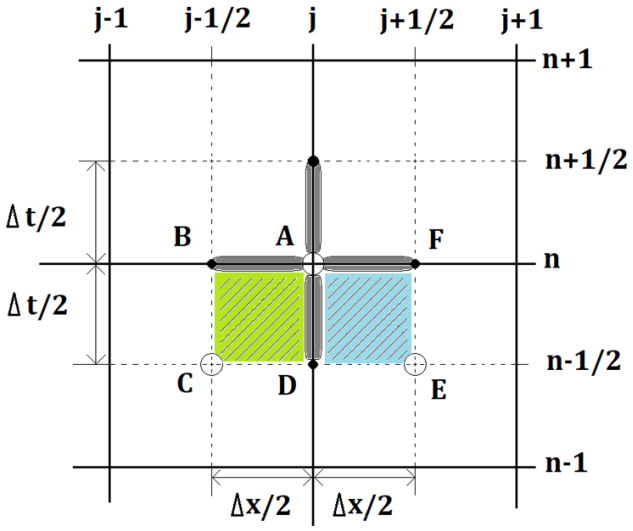

Fig. 5. The SE (solution element, gray part) and CE (conservation element, green and blue part) at position j and time n. Values at point A are calculated from points C and E at n-1/2; values at C or E are obtained from points at time n-1 via the CE and SE at the point at time n-1/2.

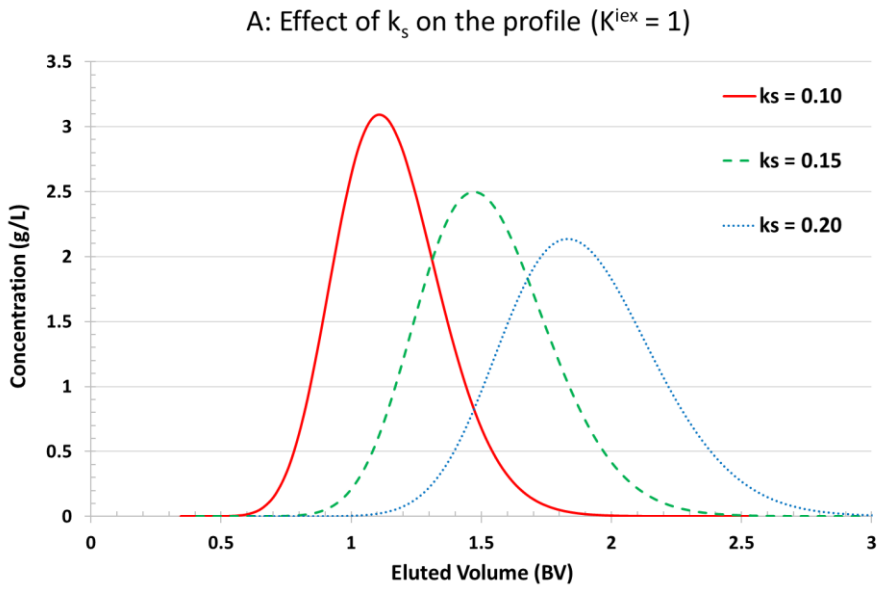

651

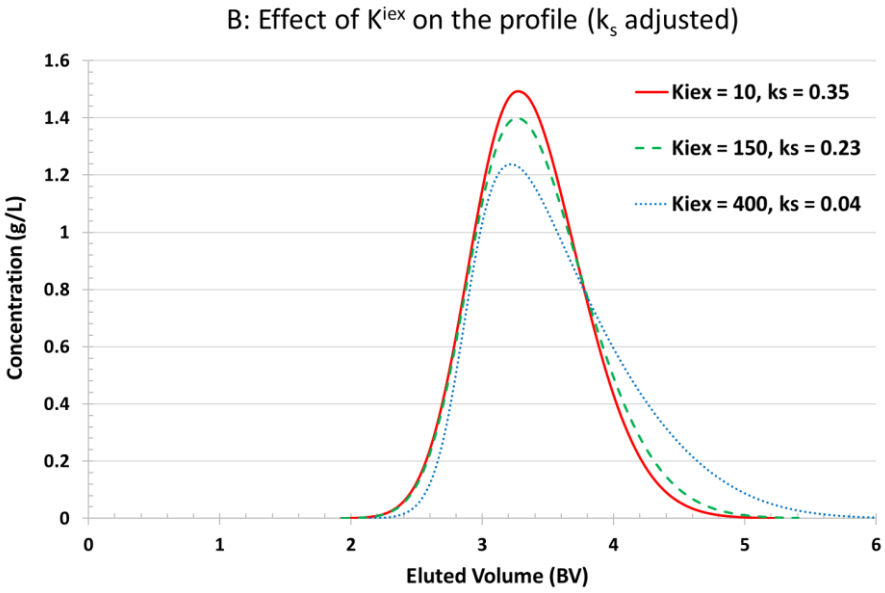

652

653 **Fig. 6.** Influence of k_s (Fig.6-A on the top) and K^{iex} (Fig.6-B at the bottom) on organic acid outlet profile.

654

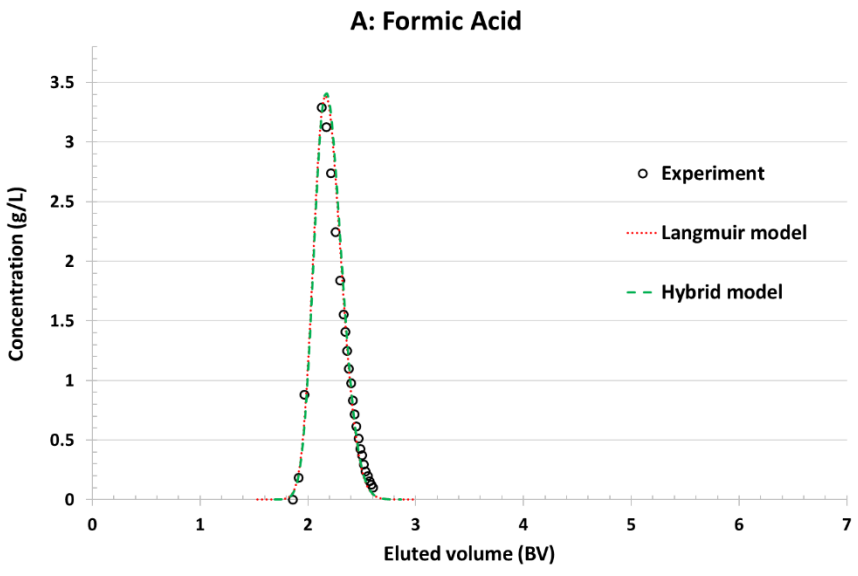

655

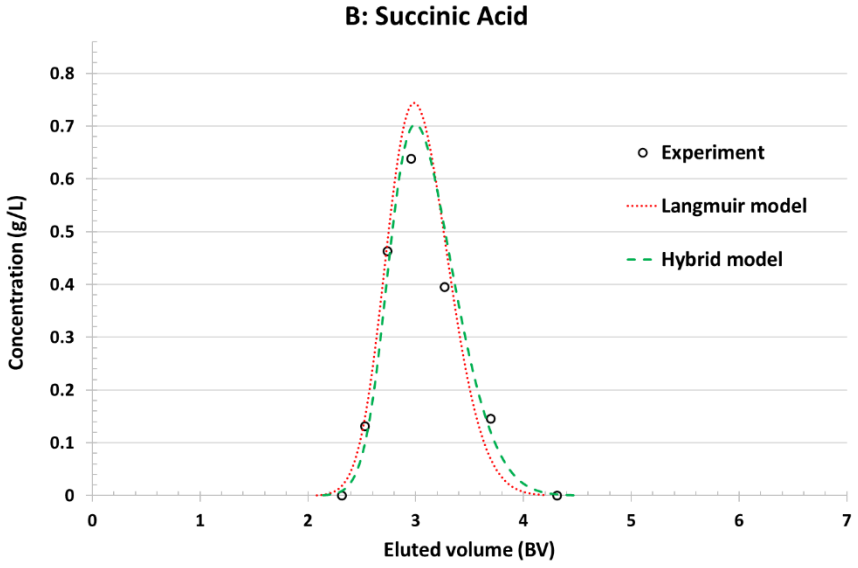

656

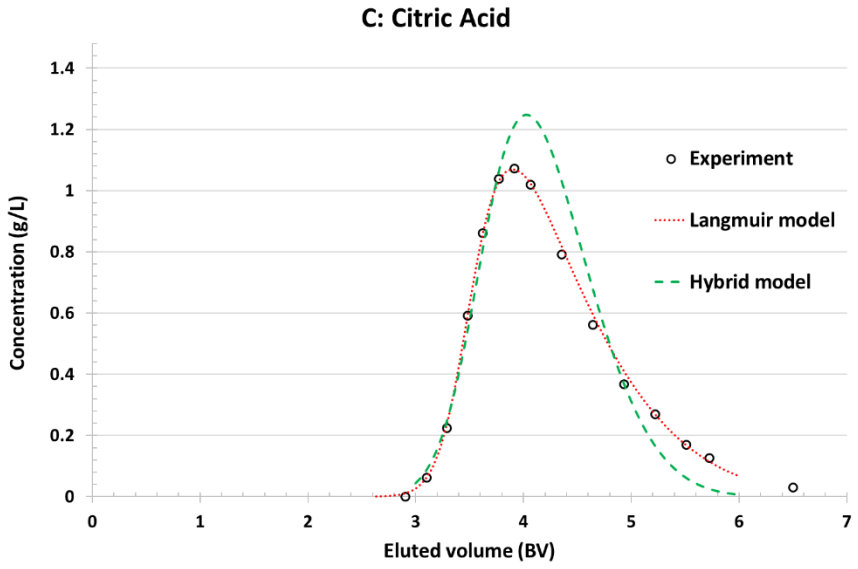

657

658 **Fig.7.** Influence of ion-exchange on outlet profile of formic (Fig. 7-A), succinic (Fig. 7-B) and citric acids (Fig. 7-C)

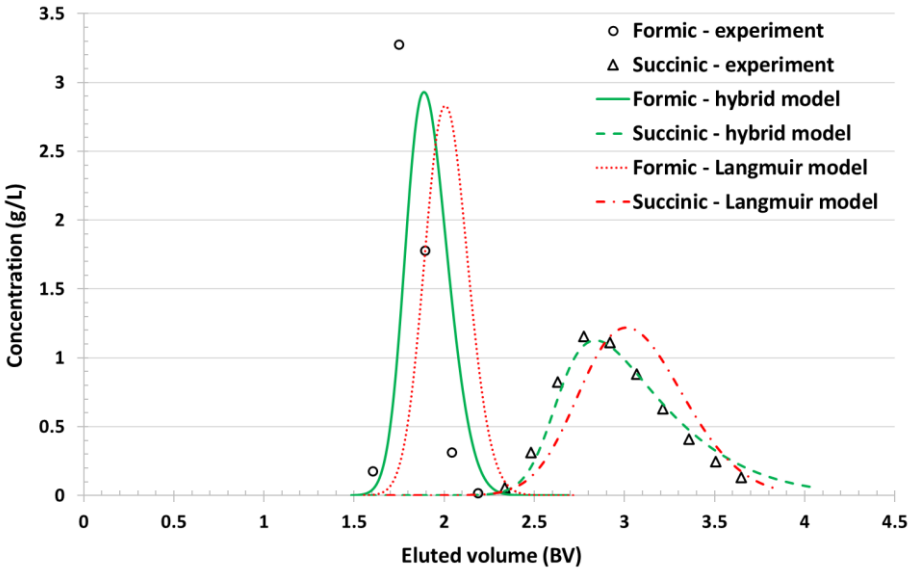

659

660 **Fig.8.** Multi-component pulse test to compare predictions of a model with only Langmuir adsorption to the
661 hybrid model, which also considers ion-exchange

662

Table 1: Chemicals used in this work

	Producer	N° CAS	Purity
Formic acid	Sigma-Aldrich	64-18-6	>98%
Succinic acid	Acros Organics	110-15-6	99%
Citric acid	Acros Organics	5949-29-1	99.5%
Sulfuric acid	VWR PROLABO	7664-93-9	95%
Na_2SO_4	Acros Organics	7757-82-6	99+%

Table 2: Devices used in this work

Device	Manufacturer	Model
Pump	MasterFlex L/S	7518-10
Column	YMC Europe ltd.	ECO25
pH/conductivity sensor	Gilson	Verity 1810
UV sensor	Gilson	159 UV-VIS
Fraction collector	Gilson	FC 203B
HPLC	Dionex	Ultimate 3000

Table 3: Main characteristics of the strong anionic resin used in this work (DIAION UMA 150)

Matrix	Styrene-DVB Gel
Functional group	Quaternary ammonium (Type I)
Salt splitting capacity	> 1.4 eq/L
Water content	37–47%
Mean particle size	220–260 µm
Uniformity coefficient	< 1.1

Table 4. Coefficients of the Langmuir equilibrium model for organic acid adsorption on HSO_4^- and SO_4^{2-} counter-anions.

Organic acids	N estimation	N assumed	k_s (L/mol)
Formic acid	0.25–1.15	0.5 or 1	0.05–0.25 (N = 0.5) 0.025–0.125 (N = 1)
Succinic acid	2.1–11	4 or 8	0.14–0.50 (N = 4) 0.07–0.25 (N = 8)
Citric acid	5.2–10	8	0.14–0.28

Table 5. Operating conditions of single component pulse tests

	Formic acid	Succinic acid	Citric acid
Sample volume (BV)	0.035	0.02	0.02
Concentration (mol/L)	0.75	0.27	0.55
Eluent	pH 1.5 H_2SO_4 (0.02 mol/L)		
Flowrate (BV/h)	0.5		

Table 6. Comparison of K^{iex} and k_s estimations of formic, succinic and citric acids

Organic acid	K^{iex} identified from pulse test	K^{iex} supplier	k_s estimated from equilibrium curves	k_s identified from pulse test simulations
Formic acid	15 ± 10	5	0.05–0.25 (N = 0.5) 0.025–0.125 (N = 1)	0.2–0.25 (N = 0.5 or 1)
Succinic acid	900 ± 100	Not given	0.14–0.50 (N = 4) 0.07–0.25 (N = 8)	0.26–0.28 (N = 4 or 8)
Citric acid	300 ± 50	250	0.14–0.28 (N = 8)	0.12–0.14 (N = 8)

Table 7. Values of k_a and D of formic, succinic and citric acids.

Organic acid	k_a van Deemter (10^{-3} s^{-1})	k_a adjusted (10^{-3} s^{-1})	D van Deemter (10^{-7} m^2/s)	D used (10^{-7} m^2/s)
Formic acid	31–35	45	1–1.1	1
Succinic acid	7.5–9.5	8	0.68–1.4	0.8
Citric acid	2.8–3.4	5.6	4–5	4

Table 8. Parameters used for multi-component pulse test simulation

Model	Organic acid	N	k_s (L/mol)	K^{iex}	k_a (s^{-1})	D (10^{-7} m^2/s)
Hybrid model (adsorption + ion-exchange)	Formic acid	0.5	0.24	25	0.045	1
	Succinic acid	4	0.26	800	0.008	0.5
Langmuir model (only adsorption)	Formic acid	0.5	0.25	0	0.045	1
	Succinic acid	4	0.44	0	0.008	0.5